

## Article

# Comparison Analysis on the Accuracy of Galileo PPP Using Different Frequency Combinations in Europe

Jia Song<sup>1</sup> and Lewen Zhao<sup>2,\*</sup>

<sup>1</sup> School of Geographic Information and Tourism, Chuzhou University, Chuzhou 239000, China; jsongwhu@whu.edu.cn

<sup>2</sup> School of Remote Sensing and Geomatics Engineering, Nanjing University of Information Science and Technology, Nanjing 210044, China

\* Correspondence: lwzhao@nuist.edu.cn

**Abstract:** The Galileo constellations are characterized by transmitting GNSS signals on multi-frequencies, which can benefit the robustness and accuracy of the solutions. However, the dual-frequency E1/E5a combinations are generally used for precise point positioning (PPP). In this paper, the performance of Galileo static and kinematic PPP using different dual- and multi-frequency combinations are assessed using observations from the European region. Overall, the accuracy of daily PPP achieved by the dual-frequency GPS, Galileo, and BDS is better than 5 mm in the horizontal direction and better than 10 mm in the vertical direction. Though the number of observed Galileo satellites is less than GPS, the horizontal accuracy can reach 1.6 mm/2.3 mm/5.7 mm on North/East/Up component, which is improved by 59.0% and 12.3% compared to the GPS in the north and up direction. Then, the accuracy of Galileo static PPP is analyzed using different dual- and multi-frequency combinations. Results indicate that the Galileo E1/E5b PPP can degrade the accuracy due to the inter-frequency clock biases between the E1/E5a and E1/E5b combinations. Best accuracy can be achieved for the triple- and four-frequency PPP, which is 4.8 mm in the up direction. The hourly accuracy for the static PPP can reach 5.6 mm/9.2 mm/12.6 mm in the north/east/up direction using the GPS/Galileo/GLONASS/BDS combinations. Finally, a positioning convergence ratio (PCR) indicator, which represents the accuracy of PPP over a period, is used to analyze the convergence time of kinematic PPP. Results indicated that the multi-frequency Galileo observations contribute minorly to the convergence of kinematic PPP. However, Galileo shows the best convergence performance for the single GNSS positioning, and the GPS/Galileo combined PPP achieved the best performance for the PPP using different GNSS combinations.



**Citation:** Song, J.; Zhao, L. Comparison Analysis on the Accuracy of Galileo PPP Using Different Frequency Combinations in Europe. *Appl. Sci.* **2021**, *11*, 10020. <https://doi.org/10.3390/app112110020>

Academic Editor: Daniele Sampietro

Received: 28 September 2021

Accepted: 19 October 2021

Published: 26 October 2021

**Publisher's Note:** MDPI stays neutral with regard to jurisdictional claims in published maps and institutional affiliations.



**Copyright:** © 2021 by the authors. Licensee MDPI, Basel, Switzerland. This article is an open access article distributed under the terms and conditions of the Creative Commons Attribution (CC BY) license (<https://creativecommons.org/licenses/by/4.0/>).

**Keywords:** Galileo; multi-frequency; precise point positioning (PPP); hourly PPP

## 1. Introduction

Precise point positioning (PPP) can achieve high positioning accuracy on regions such as mountains, deserts, or oceans without the support of external reference stations [1]. However, a long initialization period of about 30 min is still necessary for the dual-frequency kinematic PPP to achieve a reliable solution, which can be shortened to 15 min using the ambiguity-fixing method or multi-system combination [2,3]. With the modernization of the Global Navigation Satellite System (GNSS), triple- or multi-frequency signals have become available for the emerging BDS and Galileo, as well as the new generation of GPS and GLONASS satellites [4]. Therefore, the utilization of multi-GNSS and multi-frequency signals to shorten the convergence time and improve the position accuracy has been intensively investigated.

The mathematic models of PPP mainly contain the traditional ionosphere-free (IF) model and the undifferenced and uncombined (UC) model. The IF model can obtain the three-dimensional coordinates in the International Terrestrial Reference Frame (ITRF) by eliminating the first-order ionospheric delay, and it is widely used in airborne and

marine applications. In comparison, the UC model additionally estimates the ionospheric delay and can be used for ionospheric scintillation monitoring. Moreover, the UC model avoids the noise amplification and correlation between observations and can be easily extended for multi-frequency data processing. It has been demonstrated that the UC model provides the best performance if an external ionosphere model is applied [5]. However, the accuracy of the external ionospheric delay corrections is affected by the temporal and spatial characteristics of the ionosphere activity. In the regions with more active ionospheric condition (equatorial or polar regions), or during the time when solar activity level is high, global ionosphere models [6–8] cannot characterize the real ionospheric condition. To achieve high accuracy with shorter convergence time in these scenarios, accurate post-processed or real-time products should be applied [9].

The Chinese BDS-3 achieved its global constellation in 2020; results indicated that the satellite-induced code biases have been eliminated in the new constellation, and the measurement quality of BDS-3 outperforms the BDS-2 [10]. The positioning errors for static BDS PPP on a global scale were also analyzed, and they indicated that comparable performance can be achieved with respect to the GPS [11]. Moreover, the BDS-3 and Galileo constellations provide observation frequency on more than three frequencies, which bring opportunities to improve the performance of PPP. The benefits of triple-frequency observations for rapid PPP ambiguity resolution (AR) are first demonstrated by [12] based on the simulated experiment. The use of the triple-frequency BDS and Galileo observations can achieve comparable results as the dual-frequency PPP model and is not affected by the time-dependent phase hardware delays [13]. Besides, using more frequencies can improve the performance of Galileo kinematic PPP [14]. Moreover, if proper spatial and temporal ionospheric constraints are available, the triple-frequency PPP with the raw observation model can achieve better performance than the traditional dual-frequency ionospheric-free PPP [15].

The benefits of triple-frequency observations for PPP ambiguity resolution (AR) have also been analyzed. An optimal linear combination model is proposed by [16] using triple-frequency observations to improve the ambiguity resolution performance and time-to-first fix of PPP. A unified modeling strategy for triple-frequency PPP AR was proposed by [17] and indicated that the contribution of the third frequency observations can improve the float PPP solutions and the reliability of PPP AR. Concerning the contribution of more frequencies to PPP AR, E1/E5/E6 triple-frequency signals can achieve the best performance, and the use of quad- and five-frequency only bring a 1 min benefit for the Galileo PPP [18]. However, the receiver antenna phase centers of Galileo constellations are critical for ambiguity resolution when using a different third frequency combination for Galileo PPP [19].

The analysis focused on the convergence time PPP, which is critical for the kinematic PPP solutions. However, the accuracy of static PPP is important for the precise geodetic monitoring applications, which are not sufficiently analyzed. Moreover, the current method for the statistics of PPP convergence can only represent the first convergence period, which cannot indicate the accuracy of PPP afterwards. In this study, we focus on analyzing the performance of dual-frequency to five-frequency Galileo PPP and the factors affecting precision improvement. The methods of undifferenced uncombined multi-frequency PPP models are introduced in Section 2. The used datasets and the processing strategies are introduced in Sections 3.1 and 3.2. In Section 3.3, the performance of Galileo and BDS-3 PPP are first compared to that of GPS. Then, the static and kinematic performance of Galileo multi-frequency PPP is evaluated in Section 3.4. The final section provides the conclusions of the study.

## 2. Methods

The undifferenced, uncombined phase and range observation for PPP between receiver  $r$  and satellite  $s$  can be generally expressed as:

$$\begin{aligned} P_{r,f}^s &= \rho_r^s + t_r - t^s + m_r^s \cdot \delta T_r + \beta_f \cdot I_{r,1}^s + \varepsilon_P \\ L_{r,f}^s &= \rho_r^s + t_r - t^s + m_r^s \cdot \delta T_r - \beta_f \cdot I_{r,1}^s - N_{r,f}^s + \varepsilon_L \end{aligned} \quad (1)$$

where  $P_{r,f}^s$  and  $L_{r,f}^s$  are the pseudo range and carrier phase observation on frequency  $f$ ;  $\rho_r^s$  is the geometric distance from the satellite to the receiver;  $t_r$  and  $t^s$  are the receiver and satellite clock offset;  $m_r^s$  and  $\delta T_r$  are mapping function and zenith tropospheric delay parameter;  $I_{r,1}^s$  is the slant ionospheric delay on the first frequency;  $\beta_f$  is the frequency-related constant;  $N_{r,f}^s$  denotes the float ambiguities in meters;  $\varepsilon_P$  and  $\varepsilon_L$  are the unmodeled errors for the range and carrier-phase observation. Note that the precise correction models such as the relativity effects, phase-up effects, antenna phase center corrections, and ocean loading are not included in the equations but should be corrected according to the existing models.

The troposphere and the ionospheric parameters in Equation (1) are usually corrected in advance by an empirical model, then the residual errors are estimated together with other parameters with a proper epoch-wise constraint:

$$\begin{aligned} \delta T_t &= \delta T_{t-1} + \varepsilon_{T,t}, \quad \varepsilon_{T,t} \sim N(0, \sigma_T^2) \\ I_t^s &= I_{t-1}^s + \varepsilon_{I,t}, \quad \varepsilon_{I,t} \sim N(0, \sigma_I^2) \end{aligned} \quad (2)$$

where  $t$  and  $t - 1$  indicate the current and previous epoch;  $\varepsilon$  is assumed to be random errors; the corresponding variance is  $\sigma_T^2$  and  $\sigma_I^2$  for troposphere and ionosphere, respectively. If the external corrections are available to augment the PPP, the variance is important to the convergence and precision of PPP.

Note that the satellite and receiver hardware delays are not presented in the equation. The phase hardware delays can be absorbed by the ambiguity parameter. The code hardware delays can be absorbed by the ionospheric parameter and receiver clock parameter for the dual-frequency observations. However, additional inter-frequency biases should be estimated when multi-frequency observations are used. The observation model for triple-frequency PPP can be expressed as:

$$\begin{aligned} P_{r,1}^s &= \rho_r^s + t_r - t^s + m_r^s \cdot \delta T_r + \beta_1 \cdot I_{r,1}^s + \varepsilon_P \\ P_{r,2}^s &= \rho_r^s + t_r - t^s + m_r^s \cdot \delta T_r + \beta_2 \cdot I_{r,1}^s + \varepsilon_P \\ P_{r,3}^s &= \rho_r^s + t_r - t^s + m_r^s \cdot \delta T_r + \beta_3 \cdot I_{r,1}^s + IFB_r^s + \varepsilon_P \\ L_{r,1}^s &= \rho_r^s + t_r - t^s + m_r^s \cdot \delta T_r - \beta_1 \cdot I_{r,1}^s - N_{r,1}^s + \varepsilon_L \\ L_{r,2}^s &= \rho_r^s + t_r - t^s + m_r^s \cdot \delta T_r - \beta_2 \cdot I_{r,1}^s - N_{r,2}^s + \varepsilon_L \\ L_{r,3}^s &= \rho_r^s + t_r - t^s + m_r^s \cdot \delta T_r - \beta_3 \cdot I_{r,1}^s - N_{r,3}^s + \varepsilon_L \end{aligned} \quad (3)$$

The inter-frequency hardware delay parameter  $IFB_r^s$  is additionally estimated for the third frequency code observation to absorb its bias's inconsistency when compared to the dual-frequency observations.

## 3. Experiments and Results

To demonstrate the performance of Galileo PPP, observations from EUREF regional networks were processed in PPP mode. First, the accuracy of daily static PPP for Galileo and BDS dual-frequency observations were compared to that of GPS. Then, the benefits of using different frequency combinations to static PPP were evaluated. Finally, the contributions of multi-frequency observations to kinematic PPP were analyzed.

### 3.1. Processing Strategies

Data from EUREF regional network stations were selected to analyze the performance of multi-frequency PPP. The detailed processing strategies are listed in Table 1. The data

were processed based on the in-house software that is capable of real-time PPP and clock estimation. The antenna phase center (PCO) and antenna phase variations (PCV) were corrected using the IGS antenna files. There is still no official receiver antenna PCO/PCV corrections for Galileo provided, therefore, the GPS phase center corrections were used as a replacement. The corrections of the GPS L1 signal were used for the Galileo E1 signal, and the corrections of the GPS L2 signal were used for the Galileo E5a, E5b, E6, and E5 signals. As the ambiguities are resolved as float in the PPP filter, the elevation-dependent receiver PCO variations can be absorbed by the ambiguities, thus not affecting the PPP coordinate solutions [20]. Note that the products for satellite orbit/clock corrections and differential code biases (DCBs) corrections are from different centers. However, this will not affect the solution because the code hardware delays can be absorbed by the ionospheric parameters in the uncombined PPP model. The simplified elevation-dependent stochastic modeling was used for the multi-frequency PPP, assuming that there were no correlations among the different observables.

**Table 1.** Data modeling strategies for PPP.

Model	Settings
Sample rate	30 s
Elevation cutoff angle	7°
Phase wind-up	Phase wind-up correction
Satellite and receiver antenna phase center	Using igs14_2101.atx
Relativity	Corrected
Satellite attitude model	Yaw-Steering
Satellite orbit/clock	Corrected with GFZ multi-GNSS final products
DCBs	Corrected with products provided by DLR
Earth tides correction	IERS2010
Station coordinates	Estimated as static and kinematic ZHD: Saastamoinen model [21] ZWD: Estimated as the random walk process parameter for each station
Troposphere	Mapping function: Niell mapping function
Receiver clocks	Solved for at each epoch as white noise
Inter frequency bias (IFB)	Modeled as constant
Filter method	Kalman filter

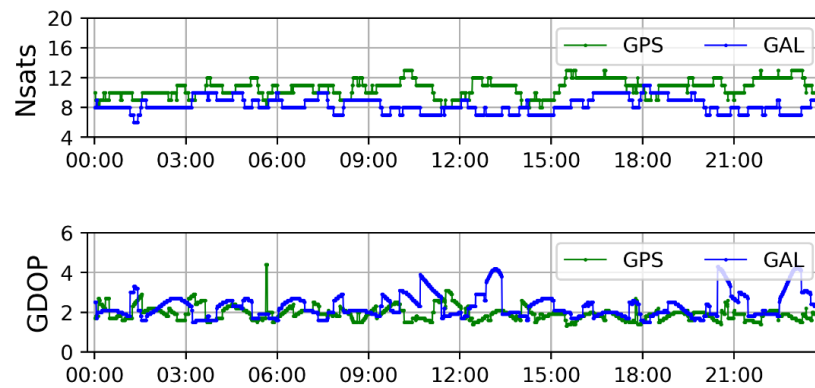
### 3.2. Evaluation of the Accuracy of Dual-Frequency Galileo Static PPP

Table 2 lists the receiver and antenna types for Galileo PPP. The stations are selected by determining that they can ensure the continuous PPP and multi-frequency observations for the selected period from the day of year (DOY) 120 to 130 in 2020. Figure 1 shows the number of available satellites and the global dilution of precision (GDOP) value for GPS and GAL at station SKE8. More than six satellites can be observed for Galileo, which is less than GPS.

The reference coordinates of the stations were collected from the EUREF weekly solution. The positioning errors are the differences between the estimated coordinates and reference coordinates. The accuracy measured by root mean square (RMS) for GPS and GAL static PPP are listed on the right panel of Figure 2, with the geographical distribution of stations shown in the left panel. The data were processed in a 24-h session, and the sampling rate was 30 s for each station. It was observed that the stations are located in the northern European area, and no obvious graphical related systematic errors were observed. The average RMS for GPS and GAL at 10 successive days are 3.9 mm/2.2 mm/6.5 mm and 1.6 mm/2.3 mm/5.7 mm on the north/east/up component, respectively. The horizontal positioning accuracy for Galileo is better than GPS, especially in the north direction, and this can be clearly observed on the right panel of Figure 2. The repeatability of RMS for station OSK6 shown in Figure 3 confirms that the repeatability of GAL PPP on the horizontal direction is better than that of GPS.

**Table 2.** Receiver types and antenna types for the Galileo tracking stations.

Receiver Type	Antenna Type	Stations
TRIMBLE NETR9	LEIAR25.R3 LEIT	ARJ6 JON6 KAD6 LOV6 NOR7 OSK6 OST6 OVE6 SKE8 LEK6
JAVAD TRE_3 DELTA	JAVRINGANT_DM SCIS	KEV2 KIV2 KILP FINS JOE2 OLK2 OUL2 ROM2 SAVU



**Figure 1.** Number of observed satellites and the global dilution of position (GDOP) for GPS and GAL on station SKE8 on DOY 120, 2020.

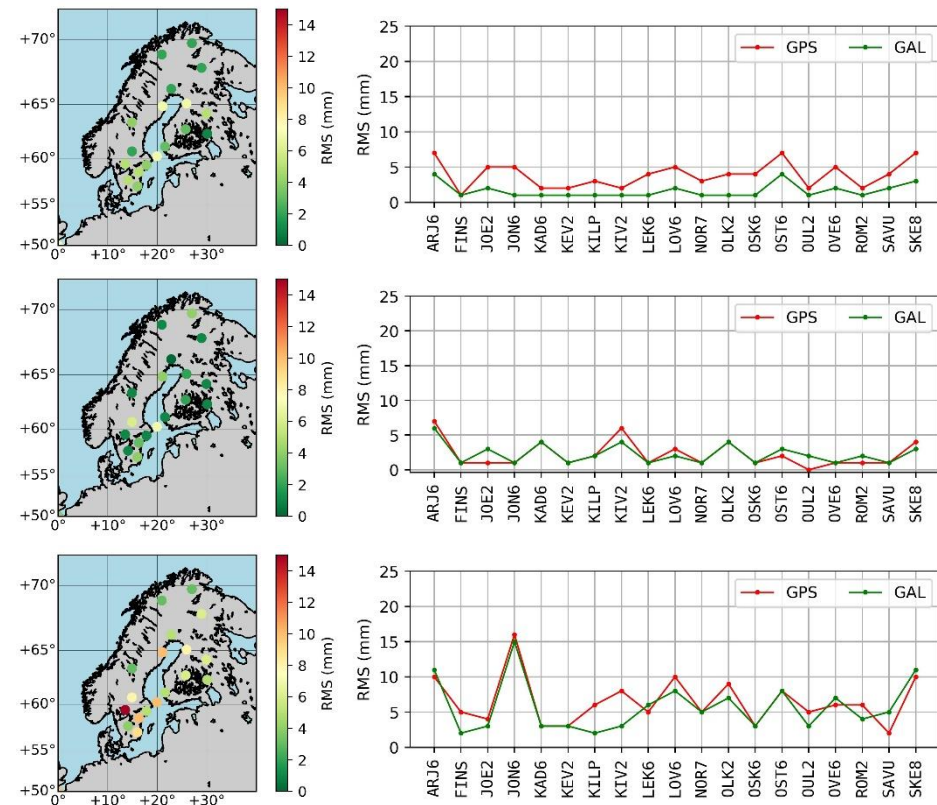


**Figure 2.** The RMS on north (top), east (middle), and up (bottom) components for GPS (left), and its comparison with the GAL dual-frequency static PPP (right).

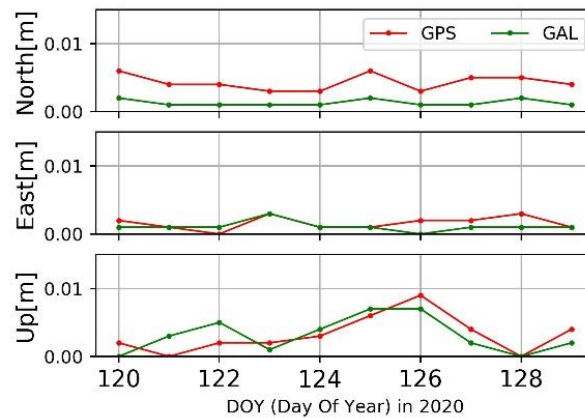


Figure 3. Repeatability of static PPP RMS for station OSK6 from DOY120 to DOY129, 2020.

Figure 4 shows the RMS of static GPS and BDS dual-frequency PPP for the selected stations. The left panel indicates the distribution of RMS, and no clear location-related distribution is observed. The right pane shows the RMS comparison of each station. The average RMS is 3.9 mm, 2.2 mm, and 6.5 mm for GPS and 2.7 mm, 2.4 mm, and 9.3 mm for BDS on the north/east/up component, respectively. The BDS can improve the RMS on the north direction by 30.7%; however, the RMS on the up direction is worse than that of GPS.

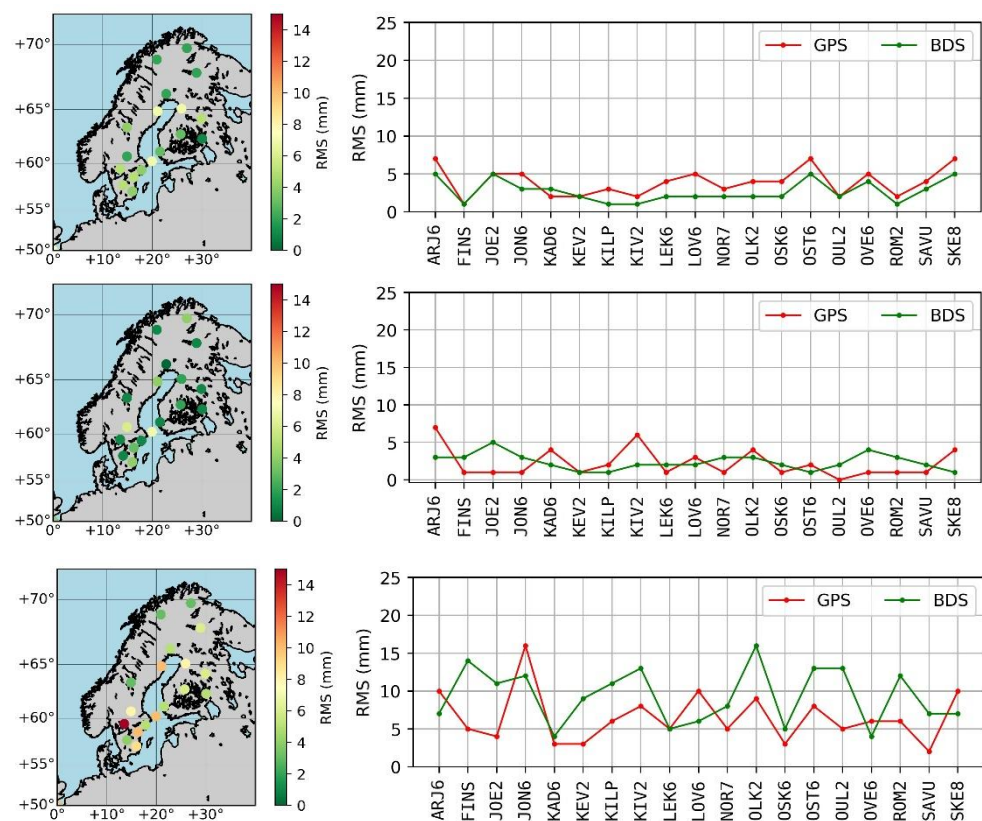


Figure 4. The RMS on north (top), east (middle), and up (bottom) component for GPS (left), and its comparison to the BDS dual-frequency PPP.

### 3.3. Evaluation of the Accuracy of Dual- and Triple-Frequency Galileo Static PPP

To evaluate the performance of different dual- and triple-frequency observations on PPP accuracy improvements, five different experiments were designed and are listed in Table 3. The multi-frequency Galileo observations were processed in the raw model and

then compared to the ionosphere-free PPP. As there are no Galileo E6 signal observations from the “TRIMBLE NETR9” receiver, it is excluded from the comparison.

**Table 3.** PPP solutions used in this study and their abbreviations.

Group	Strategies
GPS-IF	L1/L2 IF PPP
BDS-IF	B1/B3 IF PPP
GAL-IF	E1/E5a IF PPP
GAL-R15	E1/E5a RAW PPP
GAL-R17	E1/E5b RAW PPP
GAL-R18	E1/E5 RAW PPP
GAL-R157	E1/E5a/E5b RAW PPP
GAL-R1578	E1/E5a/E5b/E5 RAW PPP

Figure 5 shows the average RMS of different combinations over ten successive days. Overall, Galileo can achieve better accuracy than that of GPS and BDS PPP, with the horizontal accuracy better than 3 mm and the vertical accuracy better than 6 mm. However, there is exception for the processing mode “GAL-R17” using the E1/E5b combinations, whose positioning accuracy are observably worse than the other frequencies. It might be caused by the satellite clocks biases that exist between the E1/E5a and E1/E5b observations, which are about 0.15 ns [22]. The accuracy of PPP in the up direction can be improved when three- and four-frequency is used, reaching 4.8 mm for the triple- and four-frequency observations.

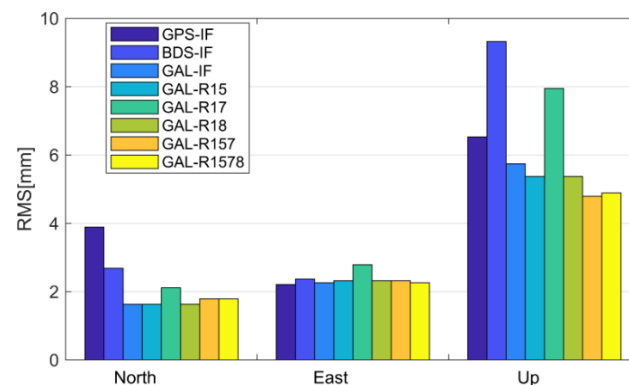


**Figure 5.** Average positioning accuracy for different observation combinations over ten days.

To characterize the site-specific reasons affecting the positioning accuracy, Figure 6 shows the average RMS of all stations in different processing options. It is observed that the accuracy in the up direction is more sensitive to the observation quality, especially for the “BDS-IF” and “GAL-R17” modes. Overall, the processing option “GAL-R18” and “GAL-R157” showed the relatively better three-dimensional accuracy.

The accuracy of hourly static PPP from different combinations were then analyzed, with a total of 4560 epochs used for the RMS statistics. Figure 7 shows the average RMS of PPP from different processing combinations. First, it was observed that the accuracy of PPP can be improved when multi-GNSS observations are used for the ionosphere-free combinations. The GPS/Galileo combinations performed better than that of the GPS/BDS combination, and the highest accuracy of 6.6 mm /8.9 mm/13.7 mm could be achieved for the “IF-GERC” multi-GNSS PPP. The raw PPP could achieve a comparable accuracy to the IF combinations, though the ionospheric-delay parameters were additionally estimated. The best positioning accuracy was achieved for the “IF-GERC” combination, reaching 5.6 mm/9.2 mm/12.6 mm on the north/east/up direction, respectively. Figure 8 shows the accuracy for different stations, and it is observed that the good accuracy of “RAW-GERC” is obvious for most stations.

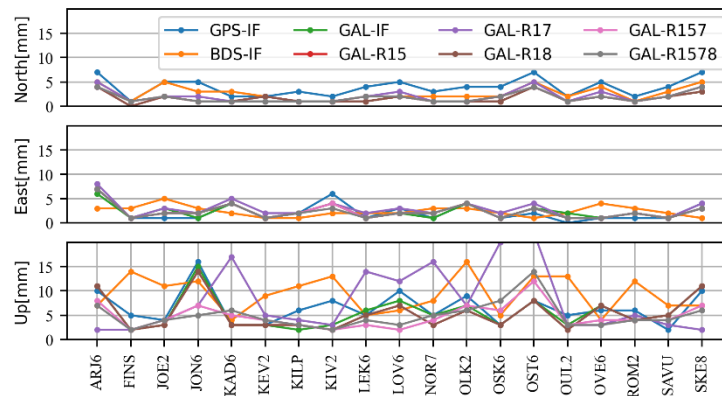


Figure 6. Site-specific RMS for different processing modes.

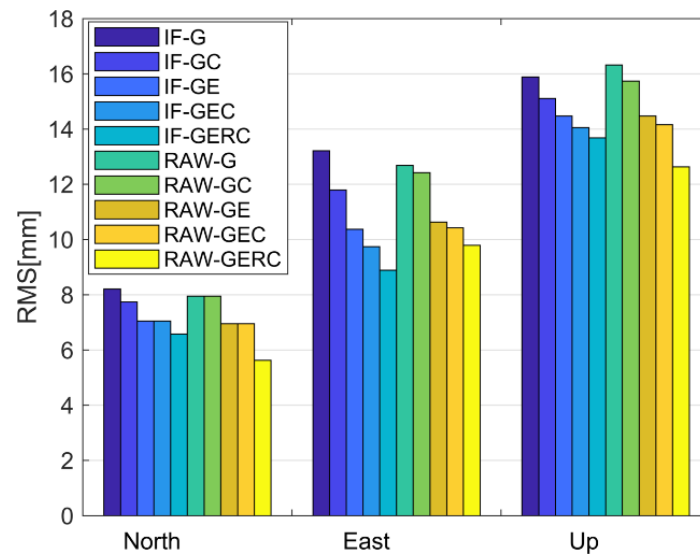


Figure 7. Average RMS of static PPP from different processing modes.

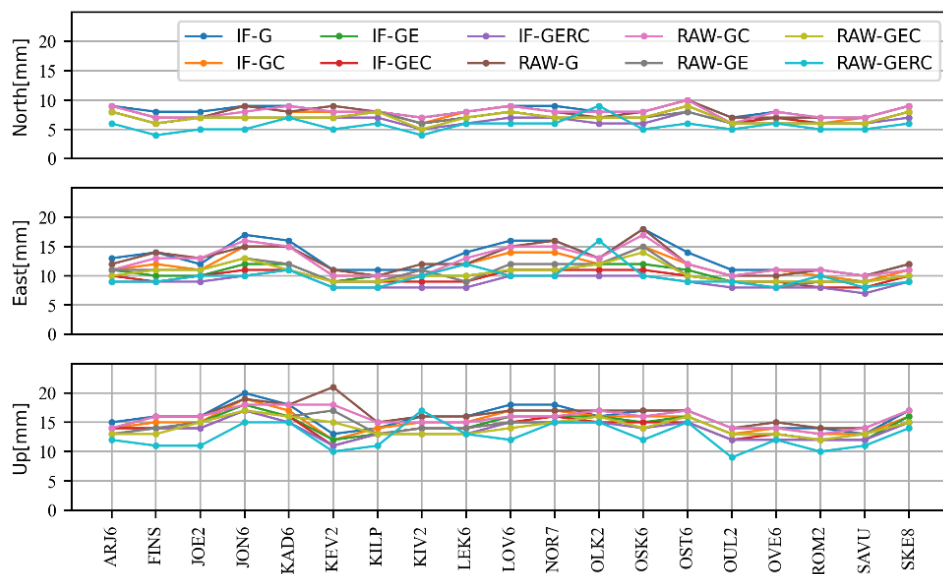


Figure 8. Average RMS of static PPP from different processing modes at different stations.

### 3.4. Accuracy of Multi-Frequency Galileo Kinematic PPP

Long convergence time is the key factor affecting the application of PPP, therefore, the contribution of multi-GNSS and multi-frequency observations to PPP convergence and accuracy improvement were assessed in the kinematic mode. Instead of calculating the convergence time using the criterion when a horizontal positioning accuracy achieves 10 cm, a positioning convergence ratio (PCR) was used to describe the accuracy improvement in different session lengths. The PCR from the starting epoch  $t_0$  to epoch  $t_0 + \Delta t$  is defined as:

$$PCR(t_0) = \frac{nConv(t_0, t_0 + \Delta t)}{nTotal(t_0, t_0 + \Delta t)} \quad (4)$$

where  $nConv$  represents the number of epochs that a horizontal positioning accuracy is less than 10 cm, and  $nTotal$  represents the total number of epochs in the session. The PPP was processed in a 1-h session, and the PCR was calculated every 5 min, i.e.,  $\Delta t = 5$  min. Using the observations from ten successive days with 30 s interval,  $nTotal$  for PCR calculations were generally 2400.

Figure 9 presents the PCR at different sessions when using single- and multi-GNSS observations. The  $x$ -axis indicates different sessions, where “S05” represents a statistical period from minute 0 to minute 5, and “S10” represents the statistical period from the minute 5 to the minute 10, and so on. It was observed that the GPS, Galileo, and BDS single constellation PPP could not achieve 100% PPP convergence accuracy, even after a 30 min convergence period, of which BDS showed poor convergence performance, followed by the GPS and Galileo constellation. Figure 10 shows the series of the positioning errors at the north, east, and up direction for GPS and Galileo kinematic PPP on station OVE6. The Galileo-only PPP showed minor errors at the convergence period. When comparing the multi-constellation combinations, the GPS + BDS performed better than that of GPS + GLONASS constellations, whereas the GPS + Galileo constellations showed the best performance. Besides, it was observed that the multi-GNSS combinations could not outperform the GPS + Galileo dual-frequency combinations, which was due to the fact that the observations at the IGS stations showed good geometry and quality. Overall, 100% convergence could be achieved after 30 min when the Galileo constellations were used.

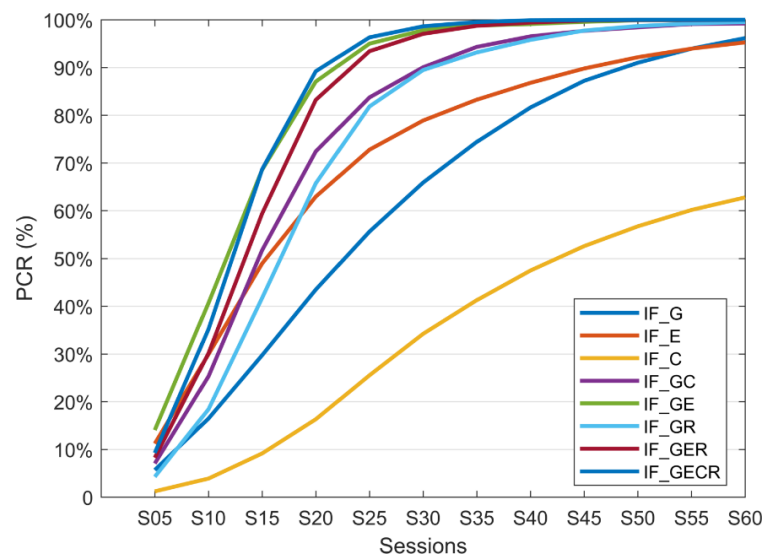


Figure 9. PCR for different GNSS combinations using the ionosphere-free combinations.

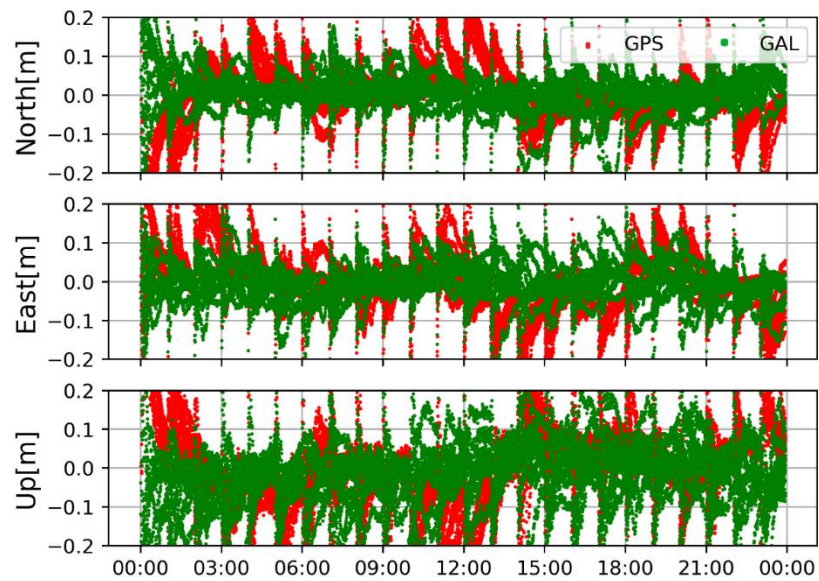


Figure 10. The positioning error series from GPS and GAL dual-frequency PPP on station OVE6.

Figure 11 shows the site-specific PCR at session “S10” and “S20” for GPS + GAL dual-frequency combinations. The data for different receiver types are separated by the red vertical line. It is observed that the stations equipped with the “JAVAD TRE\_3 DELTA” receivers showed better performance than that of the “TRIMBLE NETR9” receiver; the PCR can be improved by 30% and 14% for “S10” and “S20,” respectively. Overall, an average of 80% PCR can be achieved after 20 min and 97% can be achieved after 30 min.

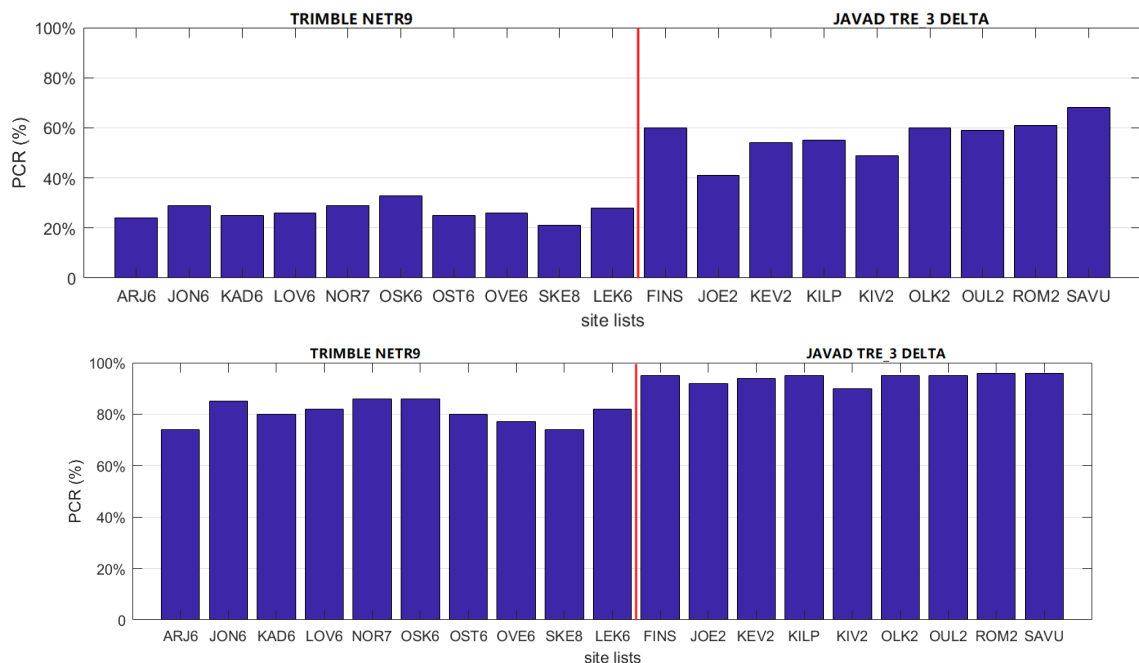
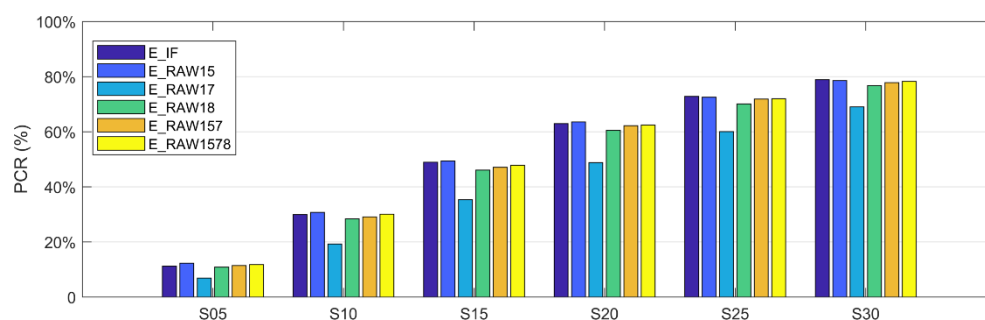


Figure 11. PCR at “S10” (top) and “S20” (bottom) for different receivers using GPS + Galileo dual-frequency PPP.

Figure 12 presents the accuracy comparison for different Galileo frequency combinations. Overall, multi-frequency combinations cannot bring improvements to the convergence of kinematic PPP. So, more efforts should focus on using multi-frequency observations to achieve fast ambiguity resolution. Specially, the convergence performance for the E1/E7 combinations were worse than the other models, which is similar to the results of static PPP in Figure 5.



**Figure 12.** PCR for different Galileo frequency combinations.

#### 4. Conclusions

The Galileo constellation has been demonstrated to have good signal quality and high precision satellite orbits/clocks products. However, the dual-frequency E1/E5a observations are generally used for the satellite clock estimation and PPP. The contribution of different frequency combinations to the static and kinematic PPP is unclear. Therefore, stations located in the European region, which is distributed with dense reference networks and promising augmented PPP service, were selected for the demonstration.

First, we compared the accuracy of dual-frequency Galileo E1/E5a PPP and BDS B1/B3 PPP with that of GPS L1/L2. Though the number of observed Galileo satellites was less than GPS, the accuracy could be improved by 59% and 12% in the north and up direction. Moreover, BDS could achieve better accuracy in the north direction than GPS, whereas the accuracy on the east and up components are worse. Overall, dual-frequency GPS, Galileo, and BDS PPP can achieve better than 5 mm accuracy in the horizontal direction and better than 10 mm in the up direction.

Then, the accuracy improvement of static PPP using additional Galileo frequencies on PPP was analyzed, including the different dual-frequency and multi-frequency combinations. Results indicated that the Galileo performs better than the GPS and BDS PPP; however, the E1/E5b combinations degrade the accuracy due to the additional frequency-induced biases. Overall, the triple- and four-frequency raw PPP can improve the accuracy in the top direction by 11%, reaching 4.8 mm. Moreover, analysis indicates that the multi-GNSS combinations can improve the accuracy of hourly static PPP, reaching 5.6 mm/9.2 mm/12.6 mm for the raw PPP model.

Finally, the convergence time and accuracy of kinematic PPP were analyzed using the PCR indicator. The single GPS and BDS PPP takes more than 30 min to achieve 80% PCR, and the performance can be greatly improved after combining the Galileo observations. Besides, the PCR are correlated with the receiver-related biases. An average 80% PCR can be achieved after 20 min and 97% can be achieved after 30 min. The Galileo kinematic PPP are also degraded by the E1/E5b observation combinations.

**Author Contributions:** J.S. completed the theoretical research and design of the manuscript and completed the writing of the manuscript. L.Z. developed the software for the PPP processing and guided the experimental process. All authors have read and agreed to the published version of the manuscript.

**Funding:** This research was funded by the Anhui Educational Commission Key Project (KJ2020A00706), the National Natural Science Foundation of China (42104018) and Natural Science Foundation of Jiangsu Province (20KJB170008).

**Institutional Review Board Statement:** Not applicable.

**Informed Consent Statement:** Not applicable.

**Data Availability Statement:** The raw GPS data are available from <https://igs.bkg.bund.de/>, (accessed on 19 October 2021). All processed GPS data during the study are available from the corresponding author by request.

**Acknowledgments:** The authors would like to thank the IGS network and EUREF network for providing the multi-GNSS data; MGEX for providing the precise orbits and biases correction files. The authors would also like to thank all anonymous reviewers for their valuable comments, which refined the present work.

**Conflicts of Interest:** The authors declare no conflict of interest.

## References

1. Zumberge, J.F.; Heflin, M.B.; Jefferson, D.C.; Watkins, M.M.; Webb, F.H. Precise point positioning for the efficient and robust analysis of GPS data from large networks. *J. Geophys. Res. Solid Earth* **1997**, *102*, 5005–5017. [[CrossRef](#)]
2. Zhao, L.; Douša, J.; Václavovic, P. Accuracy Evaluation of Ionospheric Delay from Multi-Scale Reference Networks and Its Augmentation to PPP during Low Solar Activity. *ISPRS Int. J. Geo-Inf.* **2021**, *10*, 516. [[CrossRef](#)]
3. Pan, Z.; Chai, H.; Kong, Y. Integrating multi-GNSS to improve the performance of precise point positioning. *Adv. Space Res.* **2017**, *60*, 2596–2606. [[CrossRef](#)]
4. Montenbruck, O.; Steigenberger, P.; Prange, L.; Deng, Z.; Zhao, Q.; Perosanz, F.; Romero, I.; Noll, C.; Stürze, A.; Weber, G.; et al. The Multi-GNSS Experiment (MGEX) of the International GNSS Service (IGS)—Achievements, prospects and challenges. *Adv. Space Res.* **2017**, *59*, 1671–1697. [[CrossRef](#)]
5. Teunissen, P.J.G.; Khodabandeh, A. Review and principles of PPP-RTK methods. *J. Geod.* **2015**, *89*, 217–240. [[CrossRef](#)]
6. Klobuchar, J.A. Ionospheric time-delay algorithm for single-frequency GPS users. *IEEE Trans. Aerosp. Electron. Syst.* **1987**, *23*, 325–331. [[CrossRef](#)]
7. Nava, B.; Coisson, P.; Radicella, S.M. A new version of the NeQuick ionosphere electron density model. *J. Atmos. Sol. Terr. Phys.* **2008**, *70*, 1856–1862. [[CrossRef](#)]
8. Peng, Y.; Scales, W.A.; Lin, D. GNSS-based hardware-in-the-loop simulations of spacecraft formation flying with the global ionospheric model TIEGCM. *GPS Solut.* **2021**, *25*, 65. [[CrossRef](#)]
9. Ren, X.; Chen, J.; Li, X.; Zhang, X.; Freeshah, M. Performance evaluation of real-time global ionospheric maps provided by different IGS analysis centers. *GPS Solut.* **2019**, *23*, 1–17. [[CrossRef](#)]
10. Xie, X.; Geng, T.; Zhao, Q.; Liu, J.; Wang, B. Performance of BDS-3: Measurement Quality Analysis, Precise Orbit and Clock Determination. *Sensors* **2017**, *17*, 1233. [[CrossRef](#)]
11. Jiao, G.; Song, S.; Ge, Y.; Su, K.; Liu, Y. Assessment of BeiDou-3 and multi-GNSS precise point positioning performance. *Sensors* **2019**, *19*, 2496. [[CrossRef](#)]
12. Geng, J.; Bock, Y. Triple-frequency GPS precise point positioning with rapid ambiguity resolution. *J. Geod.* **2013**, *87*, 449–460. [[CrossRef](#)]
13. Cao, X.; Li, J.; Zhang, S.; Kuang, K.; Gao, K.; Zhao, Q.; Hong, H. Uncombined precise point positioning with triple-frequency GNSS signals. *Adv. Space Res.* **2019**, *63*, 2745–2756. [[CrossRef](#)]
14. Su, K.; Jin, S.; Jiao, G. Assessment of multi-frequency global navigation satellite system precise point positioning models using GPS, BeiDou, GLONASS, Galileo and QZSS. *Meas. Sci. Technol.* **2020**, *31*, 064008. [[CrossRef](#)]
15. An, X.; Meng, X.; Jiang, W. Multi-constellation GNSS precise point positioning with multi-frequency raw observations and dual-frequency observations of ionospheric-free linear combination. *Satell. Navig.* **2020**, *1*, 1–13. [[CrossRef](#)]
16. Duong, V.; Harima, K.; Choy, S.; Laurichesse, D.; Rizos, C. An optimal linear combination model to accelerate PPP convergence using multi-frequency multi-GNSS measurements. *GPS Solut.* **2019**, *23*, 1–15. [[CrossRef](#)]
17. Xiao, G.; Li, P.; Gao, Y.; Heck, B. A Unified Model for Multi-Frequency PPP Ambiguity Resolution and Test Results with Galileo and BeiDou Triple-Frequency Observations. *Remote Sens.* **2019**, *11*, 116. [[CrossRef](#)]
18. Li, X.; Liu, G.; Li, X.; Zhou, F.; Feng, G.; Yuan, Y.; Zhang, K. Galileo PPP rapid ambiguity resolution with five-frequency observations. *GPS Solut.* **2020**, *24*, 1–13. [[CrossRef](#)]
19. Xin, S.; Geng, J.; Guo, J.; Meng, X. On the choice of the third-frequency Galileo signals in accelerating PPP ambiguity resolution in case of receiver antenna phase center errors. *Remote Sens.* **2020**, *12*, 1315. [[CrossRef](#)]
20. Zhao, L.; Václavovic, P.; Douša, J. Performance Evaluation of Troposphere Estimated from Galileo-Only Multi-Frequency Observations. *Remote Sens.* **2020**, *12*, 373. [[CrossRef](#)]
21. Saastamoinen, J. Introduction to practical computation of astronomical refraction. *Bull. Géodésique* **1972**, *46*, 383–397. [[CrossRef](#)]
22. Duan, B.; Hugentobler, U.; Selmke, I.; Wang, N. Estimating ambiguity fixed satellite orbit, integer clock and daily bias products for GPS L1/L2, L1/L5 and Galileo E1/E5a, E1/E5b signals. *J. Geod.* **2021**, *95*, 1–14. [[CrossRef](#)]